One-pot strategy for the preparation of electrically conductive composites using simultaneous reduction and grafting of graphene oxide via atom transfer radical polymerization

Monika Galeziewska[1,#], Ana Hološ[2,#], Marketa Ilcikova[2,3,*], Miroslav Mrlik[4], Josef Osicka[4], Peter Srnec[4], Matej Mičušík[2], Robert Moucka[4], Martin Cvek[4], Jaroslav Mosnáček[2,5,*], Joanna Pietrasik[1,*]

[1]*Lodz University of Technology, Department of Chemistry, Institute of Polymer and Dye Technology, Stefanowskiego 16, 90 537 Lodz, Poland*

[2]*Polymer Institute, Slovak Academy of Sciences, Dubravska cesta 9, Bratislava 845 41, Slovakia*

[3]*Tomas Bata University, Faculty of Technology, Department of Physics and Materials Engineering, Vavreckova 275, Zlin 760 01, Czech Republic*

[4]*Tomas Bata University in Zlin, University Institute, Centre of Polymer Systems, Trida T. Bati 5678, Zlin 76001, Czech Republic*

[5]*Centre for Advanced Materials Application, Slovak Academy of Sciences, Dubravska cesta 9, Bratislava 845 11, Slovakia*

[#] Authors contributed equally

For Table of Contents use only

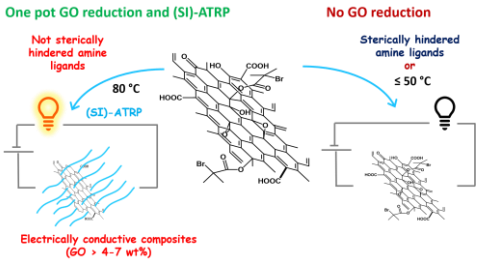

KEYWORDS: graphene oxide reduction, polymer brushes, surface-initiated polymerization, atom transfer radical polymerization, nanocomposites

ABSTRACT

In this work, a facile "one-pot" approach for the preparation of composites with tunable electrical conductivity and viscoelastic properties is presented. The effect of reaction conditions, such as reaction time and temperature as well as the structure and concentration of the tertiary amine used as a component of the catalytic complex, on the reduction of graphene oxide was investigated. The reaction conditions were optimized for simultaneous GO reduction during synthesis of two types of polymers, poly(methyl methacrylate) (PMMA) or poly(styrene–*co*-acrylonitrile) (SAN). GO-*graft*-poly(methyl methacrylate) (GO-*g*-PMMA) and GO-*graft*-poly(styrene-*co*-acrylonitrile) (GO-*g*-SAN) hybrids with electrical conductivity ranging from 10^{-8} to 10^{0} S cm^{-1} were prepared using selected tertiary amine-based ligands. Finally, the reaction conditions were adapted for *in situ* preparation of GO-*g*-PMMA/PMMA and GO-*g*-SAN/SAN composites with electrical conductivity ranging from 10^{-14} to 10^{-4} S cm^{-1}. The mechanical properties of the synthesized composites were compared with composites prepared from GO and commercial PMMA or SAN.

INTRODUCTION

Electrically conductive polymer composites (CPCs) are of enormous interest to the technology and academic worlds.[1–6] Depending on the range of electrical conductivity they can be used for various applications.[4,5,7,8] Materials with conductivity between 10^{-11} and 10^{-6} S cm^{-1} are used in electrostatic discharge (ESD) protection, e.g., fuel tanks, anti-static storage containers, mining pipes, electronic connectors, electrostatic paintable compounds, while those with electrical conductivity in the range of 10^{-6}–10^{-1} S cm^{-1} are suitable for electromagnetic interference (EMI) shielding and sensor applications, e.g., strain sensing materials, overcurrent protectors, organic liquid sensing devices, self-regulated heating elements. The last group of conductive polymer composites are highly conductive materials, with an electrical conductivity value of over 10^{-1} S cm^{-1}. They are used for applications such as conductive adhesives and coatings, thermoelectric materials, bipolar plates, resistors, busbars, etc.[4,5,7]

Graphene has been recognized as promising filler suitable for designing electrically conductive composites due to its high electrical properties. It is a two-dimensional hexagonal lattice of sp^2-hybridized carbon atoms exhibiting extraordinary thermal, mechanical, and electrical properties.[9] However, it is very difficult to obtain evenly distributed graphene in a polymer matrix because of competitive exfoliation with reaggregation of graphene sheets. Therefore, the graphene surface is modified with functional groups, mainly through the incorporation of oxygen-containing groups, which can be further modified. The obtained graphene oxide (GO) can be more homogenously dispersed in a polymer matrix. However, GO is significantly less electrically conductive than graphene.[10,11] GO may be reduced chemically or thermally to partially restore a network of sp^2 carbons and consequently increase the electrical conductivity of the GO while maintaining the improved dispersibility in a composite matrix.[10,12] There are various reducing agents that can be used for GO reduction, such as amines, metal powders, metal salts, amino acids, polyphenols, reducing sugars, and even bacteria,[10,12,13] and the reduction is usually performed before,[14,15] or after modification of the GO surface.[16,17]

Synthesis of composites in the "one-pot" approach has attracted great attention. It leads to homogenous particle dispersion and distribution within the polymer matrix and, thus, good composite performance.[18,19] Utilization of controlled polymerization techniques offers further advantages in the design of polymer architecture to more easily obtain the targeted properties.[20–26] Previously, we demonstrated that GO can be reduced in situ during surface-initiated atom transfer radical polymerization (SI-ATRP),[27,28] and this approach was applied to the synthesis of GO hybrid particles, fitting the parameters for the preparation of electrorheological fluids with potential industrial utilization.[28,29] It was recognized that two parallel processes take place during polymer synthesis from GO. In both processes a tertiary amine-based ligand, a component of the ATRP catalyst system, played a crucial role. Firstly, the ligand formed a complex with the transition metal to catalyze the polymerization, and secondly, the ligand reacted with the GO surface, leading to an increase in the electrical conductivity of the hybrid because of the GO reduction.[27]

Herein, simultaneous controlled reduction and chemical modification of GO by tethering the polymer was conducted, while the surface-initiated polymerization from GO and the polymer matrix synthesis proceeded in parallel to produce conductive composites in a "one-pot" process. The electrical conductivity of the prepared composites was tuned by selecting the appropriate ATRP and SI-ATRP conditions. First, the strategy previously used for the SI-ATRP of styrene was carefully optimized for methyl methacrylate, a monomer with a significantly higher propagation rate coefficient (k_p). Thus, GO-*graft*-poly(methyl methacrylate), GO-*g*-PMMA, and hybrids with large scales of electrical conductivities ranging from 10^{-13} S cm^{-1} to 1 S cm^{-1} were prepared. These values suggest the utilization of the generated composites in a wide range of applications, including insulation, electrostatic discharge (EDS) protection, fuel tanks, electromagnetic interference (EMI) shielding materials, sensors, conductive coatings, bipolar plates, etc.[4,8] Next, composite materials with both electrical and mechanical properties were prepared by changing the degree of polymerization of the synthesized polymers from the particles and in solution, using various filler content. Overall, the electrical and mechanical properties could be easily tuned. Finally, this "one-pot" strategy was also

used for styrene-*co*-acrylonitrile (SAN) copolymers grafted from GO and their SAN composites (SAN/GO-*g*-SAN), showing the versatility of the approach. We believe our unique strategy opens new perspectives for the preparation of well-defined functional composite materials.

EXPERIMENTAL

Materials

Graphite powder (synthetic, <20 μm) was obtained from Sigma Aldrich. Fuming nitric acid (HNO_3), potassium chlorate ($KClO_3$) and hydrochloric acid (HCl), *N,N,N*-triethylamine (TEA, ≥99%), *N,N,N′,N″,N″*-pentamethyldiethylenetriamine (PMDETA, 99%), 1,1,4,7,10,10-hexamethyltriethylenetetramine (HMTETA, 97%), tris(2-pyridylmethyl)amine (TPMA, 98%), tris [2-(dimethylamino)ethyl]amine (Me_6TREN, 97%), 4,4′-dinonyl-2,2′-dipyridyl (dNBIPY, 97%), 2,2′-bipyridyl (BIPY, ≥99%), *N,N,N*-triphenylamine (98%), *N,N,N*-tribenzylamine (99%), *N,N,N*-tributylamine (99%), *N,N*-dimethyl-*N*-butylamine (99%), *N,N*-diethyl-*N*-butylamine (97%), copper (I) chloride (CuCl, ≥99.995%), copper (I) bromide (CuBr, ≥99.999%), copper (II) chloride ($CuCl_2$, ≥99.999%), copper (II) bromide ($CuBr_2$, ≥99.999%), ethyl *α*-bromoisobutyrate (EBIB, 98%), *α*-bromoisobutyryl bromide (BiBB, 98%), ethylene bis(2-bromoisobutyrate) (2f-BiB, 97%) were supplied by Sigma Aldrich (USA). Monomers used for polymerizations: methyl methacrylate (MMA, ≥99%), styrene (St, ≥99%), acrylonitrile (AN, ≥99%) were also obtained from Sigma Aldrich (USA) and purified by passing through a column filled with basic aluminum oxide. Solvents: tetrahydrofuran (THF), *N,N*-dimethylformamide (DMF), acetone (99.5%), anisole (99%), methanol (99.8%), chloroform (98.5%), and diethyl ether (99.5%) were purchased from POCH S.A. (Poland). PMMA1 in granule form was obtained from CHiMei (Taiwan), M_n = 31,500 g mol^{-1}, M_w = 213,000 g mol^{-1}, $Đ$ = 6.67 (GPC, DMF, PMMA standard). PMMA2 was purchased from Polycasa (Czech Republic), M_n = 70,700 g mol^{-1}, M_w = 135,600 g mol^{-1}, $Đ$ = 1.92 (GPC, DMF, PMMA standard). Styrene-*co*-acrylonitrile (SAN, M_n = 61,600, M_w = 136,000 g mol^{-1}, $Đ$ = 2.2) was obtained from Sigma Aldrich in pellet form.

Graphene oxide preparation by Brodie method

The modified Brodie method[30] was used to prepare the graphene oxide. A reaction flask was charged with a magnetic stirring bar and 125 mL of fuming HNO_3 (100%) and cooled in an ice/water bath to about 0 °C. Ten grams of graphite powder was then added, and the contents of the reaction flask were stirred to obtain a homogenous dispersion. In the next step, 50 g of $KClO_3$ was gradually added to the dispersion. After complete dissolution of the $KClO_3$, the reaction flask was loosely covered with a glass stop cock to allow release of the evolved gas. The reaction mixture was stirred at 40 °C for 20 h. The reaction mixture was then poured into 1 L of deionized water (DW) and centrifuged. This step was repeated three times. The obtained GO was dispersed in 3 L of a 5% HCl solution to remove metal ions. Finally, the GO was centrifuged, washed with DW, and dried in a freeze dryer.

Graphene oxide reduction by different amines

Reduction of GO with various amines was performed as follows: The round-bottom flask (25 mL) equipped with a magnetic stir bar was filled with 100 mg GO, 6.15 mL of anisole, and one of the following ligands: PMDETA (3.50×10^{-4} mol, 0.060 g), TPMA (3.50×10^{-4} mol, 0.101 g), HMTETA (3.50×10^{-4} mol, 0.080 g), Me_6TREN (3.50×10^{-4} mol, 0.080 g), BIPY (7.00×10^{-4} mol, 0.110 g), dNBIPY (7.00×10^{-4} mol, 0.286 g), *N*,*N*-diethyl-*N*-butylamine (1.05×10^{-3} mol, 0.135 g), *N*,*N*-dimethyl-*N*-butylamine (1.05×10^{-3} mol, 0.106 g), *N*,*N*,*N*-tributylamine (1.05×10^{-3} mol, 0.194 g), *N*,*N*,*N*-triphenylamine (1.05×10^{-3} mol, 0.258 g), *N*,*N*,*N*-tribenzylamine (1.05×10^{-3} mol, 0.302 g), or *N*,*N*,*N*-triethylamine (1.05×10^{-3} mol, 0.106 g). The reaction flasks were sealed, placed in an oil bath preheated to 80 °C, and vigorously stirred for 24 h.

The effect of the reaction temperature on the reduction of GO was investigated using the same amounts of GO and anisole as above and using PMDETA (3.5×10^{-4} mol, 0.06 g), while the reaction mixture was vigorously stirred at RT, at 50 or 80 °C, for 24 h.

The effect of the tertiary amine concentration on the reduction of GO was investigated using the same amounts of GO and anisole as above and the following concentrations of PMDETA ligand: $1.4 \times 10^{-}$

^{3} mol, 0.242 g; 3.5×10^{-4} mol, 0.06 g; 8.75×10^{-5} mol, 0.0151 g; 3.5×10^{-5} mol, 0.006 g. The reaction flasks were sealed, placed in an oil bath preheated to 80 °C, and vigorously stirred for 24 h.

Reductions of the GO using PMDETA alone and PMDETA in the presence of CuBr after various reduction times were performed as follows: The round-bottom flasks (25 mL) equipped with a magnetic stir bar and filled with 100 mg GO, 6.15 mL of anisole, and either the ligand PMDETA (1.4×10^{-3} mol, 0.242 g) alone or together with CuBr (0.35×10^{-3} mol, 0.05 g) were sealed, placed in an oil bath preheated to 80 °C, and vigorously stirred for 24, 48, or 75 h.

After the reduction, the rGO samples were filtered over a 0.22 μm PTFE filter membrane and washed out with acetone (200 mL). The rGO particles were dispersed in DMF (200 mL), filtered, and washed out with acetone again. This procedure was repeated three times. Finally, the rGO was washed out with diethyl ether and place in an oven heated to 60 ℃ for 6 h.

Graphene oxide functionalization with ATRP initiator

The GO surface was functionalized with BiBB according to the procedure described in the literature.[20] Briefly, 2 g of GO powder was placed in a three-neck round-bottom flask (250 mL). Then, the reaction flask was evacuated and backfilled with argon three times. 60 mL of THF was dried over sodium wires, freshly distilled, and added to the reaction flask under argon flow. The mixture was sonicated in an ultrasound bath for 5 min to disperse the GO in the solvent. Then, 12 mL of TEA (86 mmol) was added to the reaction flask under argon flow and the mixture was cooled down to –5 °C in an ice/water bath. In the next step, 7 mL of BiBB (57 mmol) was added dropwise to the reaction mixture. The flask was sealed with a septum and kept in an inert atmosphere by a balloon filled with argon. The mixture was stirred at RT for 18 h and then heated under reflux at 80 °C for 1 h. The reaction mixture was passed through a PTFE 0.44 μm membrane to purify the reaction product, GO–Br. The obtained GO–Br was washed with 100 mL of acetone, then it was dispersed in 200 mL of DMF, sonicated for 30 s, filtered, and washed with acetone. This procedure was repeated

three times, until the filtrate was colorless. Finally, the GO–Br was washed with diethyl ether and dried in a vacuum oven at 60 °C for 12 h.

SI-ATRP from GO–Br

The general procedure of PMMA grafting from the GO–Br surface was performed as follows: A Schlenk reactor was charged with solid reagents: GO–Br (100 mg), $CuCl_2$ (0.0141 g, 0.1048 mmol) and CuCl (0.0242 g, 0.245 mmol), evacuated, and backfilled with argon 6 times. A stock solution of EBIB (291 μL, 1.984 mmol) in anisole (3 mL) and HMTETA (285 μL, 1.048 mmol) in anisole (3 mL) was prepared and bubbled with argon for 10 min. Anisole (13 mL) was placed in a separate flask and a continuous stream of argon was passed through the solvent. Then, anisole (12.95 mL), a solution of HMTETA in anisole (1.1 mL, 0.349 mmol), MMA (14.95 mL, 139.765 mmol), and a solution of EBIB in anisole (1.1 mL, 0.661 mmol) were added via a syringe to the Schlenk reactor. The polymerization was carried out at 80 °C for 48 h. The reaction was stopped by opening the reactor and diluting with acetone. The reaction product, GO-*g*-PMMA hybrid, was purified by passing through a 0.44 μm PTFE membrane and washing twice with acetone, twice with DMF, once with acetone, and once with diethyl ether. Finally, the product was collected and dried in a vacuum oven at 40 °C, 20 mbar overnight. GO-*g*-SAN hybrids were prepared using the same procedure but St and AN were used instead of MMA. CuBr, $CuBr_2$, and PMDETA were utilized instead of CuCl, $CuCl_2$, and HMTETA, respectively. In some reactions, 2f-BiB was used instead of EBIB. Combinations of reagent ratios are presented and discussed in the Results and Discussion Section.

Synthesis of composites

Polymerizations were performed using the procedure described above, but after opening the reactor and diluting the reaction mixture with acetone, the PMMA/GO-*g*-PMMA or SAN/GO-*g*-SAN composite was isolated by precipitation from the methanol. The obtained composites were

centrifuged and washed with methanol three times. Combinations of reagent ratios are presented and discussed in Results and Discussion Section.

Composite film preparation by casting from solution

The composites of the commercial material PMMA 211 and GO were prepared by casting the films from a polymer solution in the selected solvent. The PMMA (0.72g) was dissolved in chloroform (3 mL) overnight, GO (0.08 g) was dispersed in 1 mL chloroform, sonicated, and add to the dissolved matrix. The composite solution was stirred with a magnetic stirrer in a closed glass vial for 1 h, then the solution was cast on a Petri dish with a 3 cm diameter. The solvent was evaporated, then the film was dried to constant mass in a vacuum oven at 60 °C and 15 mbar.

Electrical conductivity of hybrids and composites

The hybrids were compressed at a hydraulic pressure of 7 MPa to obtain pellets with a diameter of 13 mm and a thickness of approximately 2.2–2.4 mm. The hybrids and composites with electrical conductivity lower than 10^{-5} S cm^{-1} were characterized by the two-point method: the pellets were placed between two electrodes coated with gold, and the current collected at various voltages was gathered using the highly precise Keithley 2400 SourceMeter (Keithley, USA). The electrical conductivity was calculated from the typical ohmic linear dependence. The pellets with electrical conductivity higher that 10^{-5} S cm^{-1} were measured with the four-point method according to van der Pauw using the Keithley 6517B (USA) analyzer. Three pellets of each sample were analyzed, and the average value and standard deviation were calculated.

In the case of electrical conductivity the experimental data were fitted according to percolation theory, which is described by following equations that provide a suitable mathematical description for s-shape dependency.[31] For fitting of the experimental data below the critical filler content the following equation was used, Eq. (1):

$$\sigma_{DC} = \sigma_m \left(\varphi_c - \varphi_f\right)^q \qquad (1)$$

where σ_{DC} is the measured electrical conductivity of the composites, σ_m is the electrical conductivity of the neat polymer matrix, φ_c is the critical filler volume fraction, φ_f is the volume fraction of filler, and q is the experimentally determined exponent.

Conductivity at percolation threshold is described by Eq. (2):

$$\sigma_{DC} = \sigma_f \left(\frac{\sigma_m}{\sigma_f} \right)^s \quad (2)$$

where σ_f is the electrical conductivity of the filler, and s is the experimentally determined exponent.

Finally, fitting of the experimental data above percolation threshold was performed using Eq. (3):

$$\sigma_{DC} = \sigma_0 (\varphi - \varphi_c)^t \quad (3)$$

where σ_0 is conductivity at threshold and t is the conductivity exponent.[3]

Viscoelastic property measurements

Viscoelastic investigation of the neat matrices and their corresponding composites and composites containing hybrid particles was performed using the MCR-502 Rotation Rheometer (Anton Paar, Austria). This rheometer was equipped with a Peltier cell (Anton Paar, Austria). Investigation of the improved compatibility between the filler and matrix and in situ synthesized hybrid and matrix was performed at 200 °C, from 0.05 to 50 Hz and at the linear viscoelastic region with an established strain at 2% deformation. The general characterization of the composites and matrices was performed using DMTA mode, where frequency was set to 1 Hz and 0.8% strain. The elucidated temperature range was from 25 to 200°C to determine the values of elastic and loss moduli below and above the T_g, and to investigate the shift of the T_g for various types of composites based on typical GO and GO hybrid particles.

RESULTS AND DISCUSSION

Effect of reaction conditions on the GO reduction

In our pioneer study, the tertiary amine such as PMDETA, commonly used in the ATRP of styrene as a ligand complexing a copper halide, was identified as a key player in GO reduction during ATRP.[27] It was further revealed that to obtain highly conductive hybrid particles, a long reaction time and high temperatures are necessary. Thus, designing the reaction conditions for a monomer with a low propagation rate k_p, such as styrene (k_p at 60 °C ~ 340 M^{-1} s^{-1} [32,33]), to obtain highly conductive hybrids is quite simple. The situation becomes more complex if monomers with higher k_p values, such as acrylates or methacrylates, are considered (k_p of methyl methacrylate at 60 °C ~ 820 M^{-1} s^{-1} [33,34]). It is difficult to maintain a long reaction time at a high temperature without detrimental effects, such as the coupling effect, cross-linking, or even the gel effect. To overcome this problem, the effects of various conditions, such as lower temperature, higher ligand concentration, and ligands with different activity in ATRP, were investigated.

First, the effect of reaction temperature on GO reduction was studied in the presence of 3.5×10^{-4} mol of PMDETA per 100 mg of GO in anisole as a solvent. When the reaction was performed at 80 °C the conductivity of the GO increased to about 10^{-3}–10^{-2} and 10^{0}–10^{1} S cm^{-1} after 24 and 48 h, respectively. Contrary to that, no changes in conductivity compared to neat GO were observed after 24 h reaction time, either at room temperature or at 50 °C, indicating no or negligible GO reduction. Thus, decreasing the reaction temperature with the aim of prolonging the polymerization time of monomers characterized with high k_p values clearly leads to no GO reduction. Although this was not a positive result from the viewpoint of conductive hybrid preparation or composites targeted in the current work, it provided important information about the preparation of GO-based hybrids or composites with improved mechanical properties but without the incorporation of the conductivity of the targeted material.

The effect of the PMDETA amount on GO reduction in anisole at 80 °C for 24 h is shown in Table 1. As seen, a 40-fold increase of PMDETA from 3.5×10^{-5} to 1.4×10^{-3} mol/ 100 mg of GO led to an increase in the GO conductivity of about 7 orders, from 1.7×10^{-8} to 1.35×10^{-1} S cm^{-1},

respectively. Thus, the conductivity of GO-based materials can also be modulated by the concentration of the tertiary amine-based ligand.

Table 1. Electrical conductivity of GO reduced for 24 hours using various amounts of PMDETA. The reductions were performed in anisole at 80 °C for 24 h.

Amount of PMDETA [mol] / 100 mg of GO	**Electrical conductivity, σ [S cm^{-1}]**
3.5×10^{-5}	$1.7 \times 10^{-8} \pm 0.15 \times 10^{-05}$
8.75×10^{-5}	$2.0 \times 10^{-4} \pm 0.3 \times 10^{-05}$
3.5×10^{-4}	$7.0 \times 10^{-3} \pm 0.22 \times 10^{-04}$
1.4×10^{-3}	$1.35 \times 10^{-1} \pm 0.10 \times 10^{-03}$

The activity of ATRP catalytic complexes may differ in the range of over 6 orders of magnitude with changes in the structure of tertiary amine-based ligands. Therefore, the effect of the ligand structures on the GO reduction were investigated to fix the electrical conductivity of the GO during the polymerization of various monomers without losing control of the polymerization process. As seen in Table 2, the ability of the ligands to reduce GO is dependent on the structure of the tertiary amine. While purely aliphatic tertiary amines such as Me_6TREN, PMDETA, and HMTETA provide significant reduction of GO, purely aromatic amines, such as BIPY, dNBIPY, and aromatic amines with only one aliphatic amine, such as TPMA, are not able to reduce GO. The most important observation, however, was that the ability of tertiary amine-based ligands to reduce GO is independent of the ligand activity in ATRP. Thus, in the synthesis of conductive hybrids and/or composites, one can choose aliphatic tertiary amine-based ligands with high or low activity in ATRP, based on the k_p of the monomer. Similarly, the aromatic tertiary amine-based ligands with different activity in ATRP could be chosen for monomers with various k_p values in the synthesis of nonconductive hybrids and/or composites.

Table 2 The electrical conductivity of GO upon interactions with ATRP ligands. The reductions were performed in anisole at 80 °C for 24 h. Ligand activity was arranged according to Matyjaszewski et al. [35]

Ligand	Amount of ligand [mol] / 100 mg GO	Conductivity σ [S cm^{-1}]
-	-	4.0×10^{-8}
Me_6TREN	3.5×10^{-4}	1.4×10^{-2}
TPMA	3.5×10^{-4}	1.7×10^{-8}
PMDETA	3.5×10^{-4}	7.0×10^{-3}
dNBIPY	7.0×10^{-4}	2.6×10^{-8}
HMTETA	3.5×10^{-4}	9.3×10^{-3}
BIPY	7.0×10^{-4}	1.9×10^{-8}

Increasing activity of ligands in ATRP

To better understand the effect of tertiary amine structure on GO reduction, series of simple tertiary amines were investigated (Table S1). It was found that the amines' ability to reduce GO clearly decreased with the increased chain length of the alkyl substituents on nitrogen. Thus, amines with methyl or ethyl substituents were able to reduce GO, while no GO reduction was observed in the case of tertiary amines with longer substituents, such as *N*,*N*,*N*-tributylamine, *N*,*N*,*N*-triphenylamine, or *N*,*N*,*N*-tribenzylamine, because of the high steric hinderance effect of the substituents, which prevented the involvement of nitrogen in the reduction process. This was in good agreement with the ability of the tertiary amine-based ligands studied above, where only those bearing methyl substituents reduced the GO surface.

We expected that the reduction of the GO by tertiary amines could proceed after nucleophilic attack on carbons bearing hydroxyl or epoxide groups, with subsequent dehydration and restoring of double bonds on the GO surface (Scheme 1). It is well-known that the nucleophilicity of the amines is affected by the steric hinderance effect of the substituents. In addition, thermal decarboxylation can proceed at the GO edges. It should be noted, however, that only the reduction mechanism shown in Scheme 1 can lead to the recovery of a conjugated graphene-like structure accompanied by a significant increase in electrical conductivity. The simultaneous process of reduction and decarboxylation cannot be ruled out. For better insight into the process, the chemical structure of GO

and the structural changes on the GO surface during the reduction with PMDETA alone or in the presence of the PMDETA/CuBr mixture were investigated by XPS.

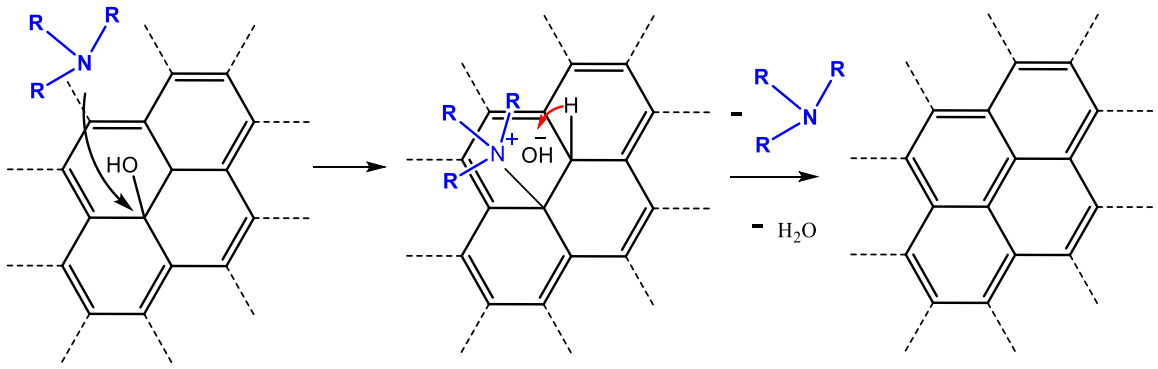

Scheme 1. Proposed reduction of GO by tertiary amines through nucleophilic attack of carbons bearing hydroxyl (or epoxide) groups with subsequent dehydration and restoration of double bonds on the GO surface.

As shown in Table 3, besides carbon (C1s signal at ca. 285 eV), in GO there were detected oxygen (O1s signal at ca. 532 eV), nitrogen (N1s signal at ca. 400 eV), and chlorine (Cl 2p signal at ca. 199 eV), probably from the preparation method of GO. When CuBr was used the $Cu2p_{3/2}$ signal centered at ca. 934.2 eV was detected, corresponding to Cu^{2+} species.[36] C1s spectra exhibited a signal at ca. 284.4 eV, corresponding to sp^2 carbon, and satellite feature (π-π^*) at ca. 290.5 eV, corresponding to delocalized conduction π electrons. This signal represented GO or rGO platform. Other C1s signals, namely, sp^3 (285.0 eV), C–O (286.6 eV), C=O (288.4 eV), and OC=O (288.8 eV), could be attributed to the oxidation on the surface. C–O centered at ca. 286.6 eV is a typical peak for GO and in this case could have overlapped with the C–N signal coming from PMDETA.

As seen from Table 3, the graphene oxidation procedure used herein provided approximately 2 at % of carbon in the form of carbonyl and carboxyl groups. Their content was within the margin of error for the reduction of GO, indicating no or negligible extent of decarboxylation. In contrast, a significant decrease in C1s C-O component, assigned to carbon bonded to hydroxyl or epoxy groups, from 60 at % down to about 30 at %, was observed after the reduction using PMDETA alone.

Similarly, a decrease in the C1 sp^3 component to about half was observed after 24 h of reduction, with only a slight further decrease after prolonged reduction for 48 h. This was accompanied by a dramatic increase in the C1s sp^2 component. At the same time, an increase in the C/O ratio from approximately 2.8 for GO to 5.2 and 6.2 after reduction for 24 and 48 h, respectively, was observed. To clearly observe the reduction effect, the surface chemical composition was plotted in Figure S1.

Table 3. Apparent surface chemical composition of prepared samples as determined by XPS. GO samples before and after reduction for various time using either PMDETA alone or PMDETA in the presence of CuBr (CuBr:PMDETA = 1:4) are compared.

Sample	Surface chemical composition [at %]				
	C1s **sp^2/sp^3/C-O/C=O+OCO/π-π***	**O1s**	**N1s**	**Cl2p**	**$Cu2p_{3/2}$**
GO	72.9 3.4/33.6/60.0/2.1/1.0	25.7	1.2	0.3	—
GO 24h PMDETA	81.7 43.8/17.7/34.0/2.3/2.2	15.8	2.3	0.2	—
GO 48h PMDETA	83.7 48.9/16.7/30.3/1.7/2.4	13.5	2.6	0.2	—
GO 24h PMDETA/$CuBr_2$	73.7 11.4/37.9/48.4/1.5/0.9	21.2	4.2	0.3	0.6
GO 48h PMDETA/$CuBr_2$	75.4 21.3/31.9/44.3/1.2/1.2	18.7	4.3	0.3	0.7
GO 75h PMDETA/$CuBr_2$	77.6 28.3/28.1/40.0/1.7/2.0	17.5	4.1	0.2	0.5

As already mentioned, during the ATRP in the presence of GO, the ligand was involved in both processes, i.e., reduction of GO and complexation with the copper salt to form the ATRP catalyst. These two processes were expected to be competitive; therefore, the XPS was used to follow the structural changes in the presence of 0.25 equivalent amount of CuBr to the PMDETA ligand.

After 75 h of reduction the C1s C-O component decreased only to about 40%. Similarly, the C/O ratio increased only to 4.4, and a lower increase was observed in the case of the C1s sp^2 component. Interestingly, the C1s sp3 component first increased from 33.6 to 37.9% after 24 h of reduction with the PMDETA/CuBr system. At the same time, more nitrogen and copper were detected in the sample, probably due to interactions of the CuBr/PMDETA complex with the GO surface. Increased

PMDETA content on the GO surface could have contributed to a slight increase in the C1 sp^3 component. With prolonged reduction time, the content of nitrogen retained almost the same, while the progressive reduction of the GO surface led to a decrease in the C1s sp^3 component to 31.9 and 28.1% after 48 and 75 h of reduction, respectively.

It was concluded, therefore, that the presence of CuBr significantly slowed down the GO reduction process because part of the PMDETA was complexed with CuBr and thus no longer contributed to the GO reduction. This observation was considered when planning further experiments.

Synthesis of electrically conductive GO-g-PMMA/PMMA composites

Me_6TREN, PMDETA, and HMTETA were identified as the ligands efficient in the GO reduction. As Me_6TREN is too active for the polymerization of methyl methacrylate,[37] attention was paid to the latter two ligands. The polymerization performed under normal ATRP conditions using a 4-fold excess of PMDETA provided high monomer conversion in only 2.5 h with formation of well-defined PMMA, while, as expected, the separated GO-*g*-PMMA hybrids showed only negligible enhancement of electrical conductivity compared to neat GO (Table 4, Entry A1). To enhance the conductivity of GO-*g*-PMMA, the reaction was slowed by using HMTETA instead of PMDETA. The equilibrium coefficient $K_{ATRP} \sim 10^{-8}$ in that case was one order of magnitude smaller than for PMDETA, $K_{ATRP} \sim 10^{-7}$.[38] Additionally, CuCl was used instead of CuBr, because CuCl typically results in slower polymerization.[39] The utilization of a catalytic system with equimolar amounts of HMTETA to CuCl led to 56% monomer conversion after 6 h (Table 4, Entry A2) with only a slight enhancement of the conductivity of the hybrids. The efficiency improvement of the GO reduction by addition of an excess of cheap Et_3N was not successful, and only a slight acceleration of polymerization was obtained (Table 4, Entry A3), probably from either allowing more HMTETA to be involved in ATRP process or using Et_3N as a reducing agent for the copper catalyst[40] and thus increasing the concentration of growing radicals in the system.

Therefore, the reaction system without Et_3N was run for longer times (Table 4, Entries A4–A6). After 48 h, an almost complete monomer conversion was reached while low dispersity was retained (Figure S2). The conductivity of the GO-*g*-PMMA progressively increased to 2.8×10^{-3}, 4.3×10^{-1}, and 4.6 S cm^{-1} after 24, 48, and 66 h of polymerization, respectively.

Table 4. Molar ratios of reagents, reaction conditions, monomer conversion determined by ^1H NMR; numbers of average molar mass (M_n) and dispersity ($Đ$) determined by the GPC of free polymers and electrical conductivity of the prepared hybrids. In all reactions (except Entry A1) $CuCl/CuCl_2$/HMTETA was used as a catalytic system, 50 vol % of anisole as solvent was used, and unless otherwise mentioned reaction, 3.50×10^{-4} mol HMTETA/100 mg GO–Br was used and the reaction temperature was 80 °C.

Entry	Molar ratios MMA:EBiB:CuX:CuX_2:L	GO–Br [wt %]	Time [h]	Conv. [%]	M_n [g mol^{-1}]	$Đ$	Electrical conductivity [S cm^{-1}]
A1[a]	100:1:0.9:0.1:4	6.3	2.5	91	8,800	1.2	$1.3x10^{-8}$ $\pm4.7x10^{-10}$
A2	210:1:0.5:0.35:0.5	0.7	6	56	10,300	1.10	$1.2x10^{-7}$ $\pm2.2x10^{-9}$
A3[b]	210:1:0.35:0.15:0.5	0.7	6	76	15,200	1.10	$4.9x10^{-7}$ $\pm5.6x10^{-9}$
A4	210:1:0.35:0.15:0.5	0.7	24	68	17,000	1.09	$2.8x10^{-3}$ $\pm3.8x10^{-5}$
A5	210:1:0.35:0.15:0.5	0.7	48	97	21,000	1.16	0.43±0.04
A6	158:1:0.35:0.15:0.5	0.9	66	94	17,900	1.11	4.57±0.04

[a] $CuBr/CuBr_2$/PMDETA was used as the catalytic system and polymerization temperature was 60 °C, 5.88×10^{-4} mol PMDETA/100 mg GO–Br; [b] Et_3N was used in addition to HMTETA in a molar ratio of 10:0.5

The reaction conditions were subsequently adopted for the preparation of composites with various GO-*g*-PMMA hybrid contents to find the percolation threshold for the GO-*g*-PMMA/PMMA composites. The composites were prepared by simultaneous polymerization of MMA from both initiators covalently attached on the GO-surface and sacrificial initiators. The list of the composites and their basic characterizations is shown in Table 5. It is worth mentioning that determination of the

exact content of either GO or GO-*g*-PMMA in the PMMA composite was complicated because of the simultaneous reduction of GO and grafting of the GO surface by PMMA chains. The approximate content of GO-based filler in GO-*g*-PMMA/PMMA composites was calculated from feed GO content and monomer conversion (determined by ^{1}H NMR). In Entry B1 (Table 5) the monomer conversion was 91% and the filler content was recalculated to 0.77 wt % compared to 0.7 wt % of the feed GO content. The monomer conversions for Entries B2–B6 (Table 5) were almost quantitative; therefore, the filler content in the composites was considered the same as the feed content of GO, i.e., approximately 3, 5, 6, 7, and 10 wt %.

Upon reaching the percolation limit of the filler, the charge moved over the composite film through conductive pathways provided by the conductive particles. The polymer brushes prevent the charge transport in the case of high grafting density and long polymer chains. For example, for poly(cyclohexyl methacrylate) the limit for the charge transport was at a molar mass of 100,000 g mol^{-1} and grafting density of 0.14 chains nm^{-2}.[41] The longer chains grafted from carbon nanotubes resulted in a thick polymer shell that increased the internanotube distance over 20 nm. Due to that the charge transport via hopping or tunneling mechanism was not allowed.[41] Therefore, the molar mass of the grafted chains shown in Table 5 (Entries B1–B6) was kept rather low; the maximal molar mass was 22,000 g mol^{-1} for Entry B1 and for Entries B2–B6 it was in the range of ~5,000–8,000 g mol^{-1}. The thickness of the grafted layer was thus small and enabled the charge transport. The electrical conductivity of the synthesized composites was measured by the four-point method in the case of materials exceeding the electrical conductivity of 1.10^{-6} S cm^{-1}. The results are shown in Table 5. For non-conducting samples the two-point method was used for comparison (see Table S2). The composite containing 5 wt % was at the percolation threshold. The electrical percolation is depicted in Figure 1.

Table 5. Molar ratios of reagents, reaction conditions, monomer conversion determined by ^{1}H NMR; numbers of average molar mass (M_n) and dispersity ($Đ$) determined by GPC of free polymers; filler content and electrical conductivity of the prepared composites. In all reactions CuCl:$CuCl_2$ in a molar ratio of 0.35:0.15 was used at a temperature of 80 °C; 50 vol % of anisole as solvent and 3.50×10^{-4} mol HMTETA/100 mg GO–Br were used in all reactions.

Entry	Molar ratios			GO–Br [wt %]	Time [h]	Conv. [%]	M_n [g mol^{-1}]	$Đ$	Filler content [wt %]	Electrical conductivity [S cm^{-1}]
	MMA	I	Cu:L							
B1	210	1[a]	0.5:0.5	0.7	48	91	21,800	1.13	0.77	$4.4\text{x}10^{-14}$ $\pm5.3.0\text{x}10^{-16}$
B2	48	1[a]	0.5:0.5	3.0	48	>99	7,000	1.20	3.0	$9.4\text{x}10^{-14}$ $\pm6.1\text{x}10^{-16}$
B3[a]	26	1[a]	0.5:0.5	5.0	48	>99	4,900	1.24	5.0	$7.8\text{x}10^{-6}\pm$ $4.0\text{x}10^{-7}$
B4	50	1[a]	0.5:1	5.6	48	>99	8,100	1.29	5.6	$2.4\text{x}10^{-7}\pm$ $3.3\text{x}10^{-8}$
B5	52	1[a]	0.58:1.5	7.3	48	>99	7,400	1.29	7.3	$8.2\text{x}10^{-6}$ $\pm1.5\text{x}10^{-7}$
B6	56	1[a]	0.6:2	9.9	48	>99	7,700	1.23	9.9	$4.0\text{x}10^{-4}\pm$ $2.0\text{x}10^{-6}$
B7	667	1[b]	1.7:26	9.9	68	92	70,500	1.34	10.7	$1.8\text{x}10^{-5}$ $\pm1.1\text{x}10^{-7}$
B8	667	1[b]	1.7:26	9.9	69	84	65,700	1.32	11.6	$8.7\text{x}10^{-4}$ $\pm4.1\text{x}10^{-6}$
B9	225	1[b]	1.25:19	9.9	72	99	44,200	1.18	10.0	$7.4\text{x}10^{-5}$ $\pm2.4\text{x}10^{-7}$
B10	169	1[b]	0.46:6.5	9.9	72	96	33,700	1.17	10.3	$7.5\text{x}10^{-5}$ $\pm6.4\text{x}10^{-7}$
B11	169	1[b]	0.46:6.5	14.2	192	>99	36,000	1.28	14.2	$9.9\text{x}10^{-4}$ $\pm3.7\text{x}10^{-6}$

I stands for free initiator, namely, [a] EBIB, [b] 2f-BiB—the molar ratio is related to the molar content of bromide groups

To evaluate the percolation threshold, Equations (1)–(3) were used for fitting and the following calculations. As one of the crucial parameters the conductivity of the matrix was calculated to be 2.17×10^{-14} S cm^{-1}. This was in good agreement with the conductivity of 1.1×10^{-14} S cm^{-1} experimentally determined for the pure PMMA matrix. Another critical parameter calculated from the percolation equations was conductivity of the filler, equal to 0.918 S cm^{-1}. That again corresponded well to the experimentally measured conductivity of the GO-*g*-PMMA hybrid filler

isolated directly from the composite B9 showing a conductivity of 0.326 S cm^{-1}. The density of the neat GO was measured and calculated, providing the value of approximately 2.49 g cm^{-3}. In contrast, the density of the hybrids was determined to be 1.59 g cm^{-3}. Using this density, the most important parameter, the critical filler content of the percolation threshold was found to be 2.39 vol %, which corresponds to 3.8 wt %.

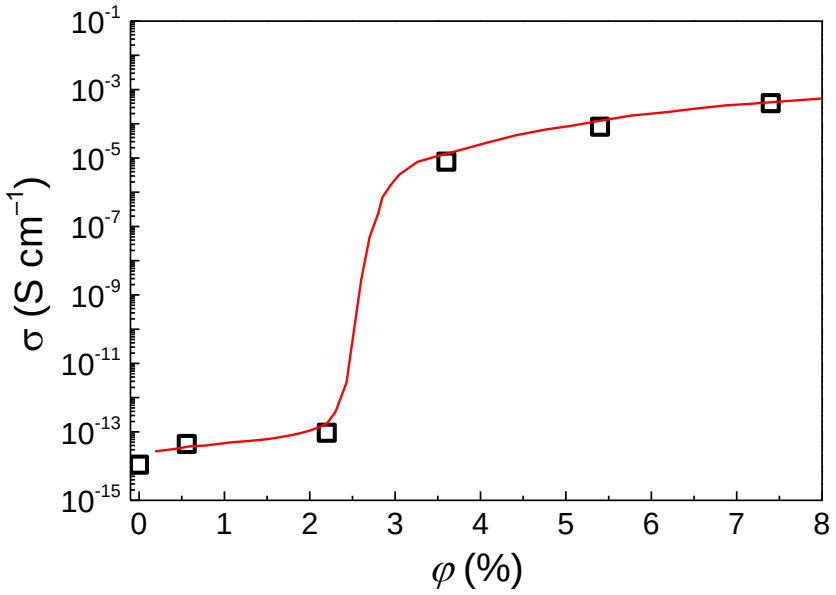

Figure 1. Dependence of the electrical conductivity on the volume fraction of the composites containing hybrid GO particles. The red line represents electrical percolation model fit. Error bars for electric conductivity are not higher than the size of the square symbols.

To prepare composites that are electrically conductive and show good mechanical properties, the molar mass of PMMA chains was further tuned. The molar mass of the grafted PMMA chains is tuned by setting the monomer to initiating alkyl bromide groups. At the same time, the molar mass of the PMMA chains of the matrix is doubled compared to the grafted ones using a bifunctional sacrificial initiator. Even though X. Gao et al.[42] suggested based on the modeling that the molar mass of grafted polymer chains is slightly higher than the one grown from sacrificial initiator, the use of the bifunctional sacrificial initiator ensures minimal effect of the small deviation in the molar mass

of grafted polymer chains on final mechanical properties. Moreover, as shown above, small difference in molar mass should not have significant effect on conductivity properties. Thus, in subsequent studies the molar mass of free PMMA chains was targeted to be in the range of 30–70 kg mol^{-1} (see Table 5, Entries B7–B11). The effect of the molar mass of the grafted PMMA chains (expected to be half of the free PMMA chains) as well as of the reaction time on the electrical conductivity of the composites was further investigated. The composites containing a comparable amount of filler, approximately 10 wt % of the filler, were prepared. As can be seen from Table 5 (Entries B6–B11), comparable electrical conductivities were determined for all prepared GO-*g*-PMMA/PMMA composites based almost entirely on the length of the grafted PMMA chains within the investigated molar mass range of 7,700–36,000 g mol^{-1}. This clearly confirmed that in such a range of PMMA chain lengths the polymer shell on the GO surface was sufficiently thin to avoid any negative effect on the conductive network formation.

Viscoelastic properties of GO-g-PMMA/PMMA composites

The effect of the molar mass of the PMMA chains on the viscoelastic properties of the composites was investigated by melt rheology at 200 °C in a frequency sweep (Figure 2). The basic rheological parameters, such as frequency dependence of complex viscosity (η^*), storage modulus (G'), and loss modulus (G''), were characterized. The η^* clearly decreased with the molar mass of the PMMA chains (Figure 2a). Composites B7 and B9 both contain 10 wt % of GO, while the M_n of free PMMA was 77,500 and 44,200 g mol^{-1} for B7 and B9, respectively. The η^* decreased progressively with increased frequency, while the higher values were observed in B7 because of the longer chain PMMA chains. A different shape was observed in the B11 composite. It contained a higher amount of GO, 14.2 wt %, and the M_n of freely dispersed PMMA chains was 36,000 g mol^{-1}; therefore, the complex viscosity reached the highest values in the high frequency region. On the other hand, at low frequencies the highest viscosity was observed in the system with the longest free PMMA chains, B7, which points to the highest number of entanglements in the system.

This is also confirmed in Figure 2b, where the crossover point (COP) of storage (*G'*) and loss modulus (*G''*) are plotted. Above the COP the storage modulus overcame the loss modulus, i.e., the solid-like behavior predominated over liquid-like behavior. With the increasing M_n of the PMMA chains the material behaved more like a solid, and the COP shifted to lower frequencies. While B11 (M_n of freely dispersed PMMA chains 36,000 g mol^{-1}) showed the COP at 4.2 Hz, the composites B9 (M_n = 44,200 g mol^{-1}) and B7 (M_n = 77,200 g mol^{-1}) showed the COP at 0.8 and 0.3 Hz, respectively.

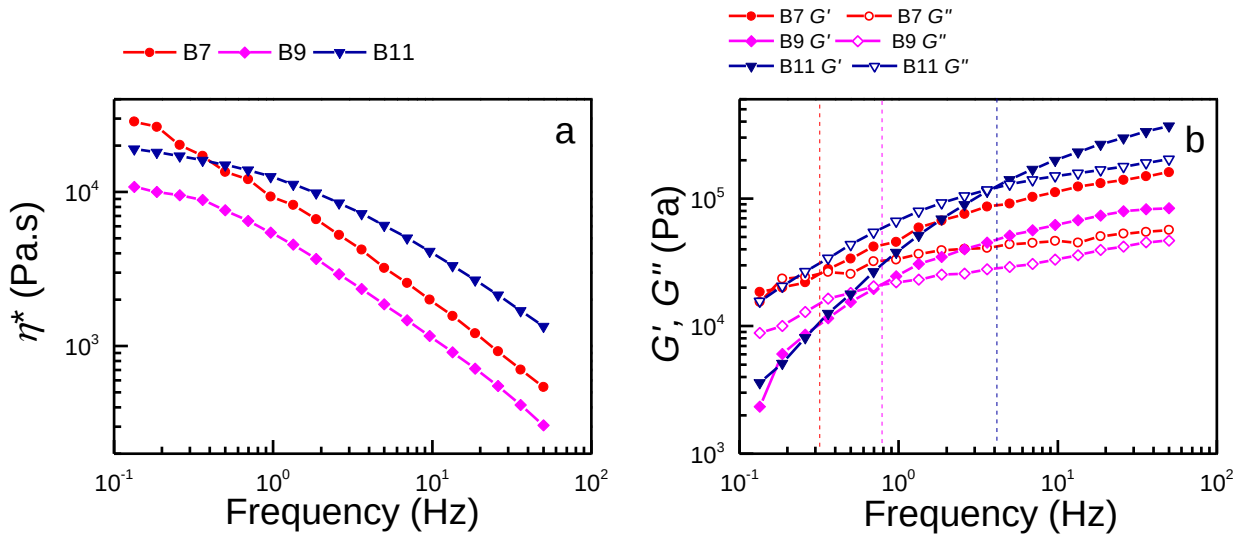

Figure 2. The viscoelastic properties of GO-*g*-PMMA/PMMA composites B7, B9, and B11 investigated at 200 °C, (**a**) frequency dependence of complex viscosity, (**b**) crossover point of storage (solid symbols) and loss modulus (open symbols).

To quantify the interactions of the GO-*g*-PMMA hybrids with the PMMA matrix chains the data were fitted with the Cole–Cole model (4), which is sensitive to polymer backbone architecture, molecular weight, and dispersity, and enables analysis of the relaxation times of the polymer chain.[43,44] The variation of viscosity components (η''versus η') was fitted with the model in the following form:

$$\eta^*(\omega) = \frac{\eta_0}{1 + (i\omega\lambda_0)^{1-h}} \qquad (4)$$

where $\eta^*(\omega) = \eta'(\omega) - i\eta''(\omega)$ is the complex dynamic viscosity, η_0 is the zero-shear viscosity, ω is the angular frequency, λ_0 is a characteristic relaxation time, h is a dispersion parameter, and i is the imaginary number ($i^2 = -1$).

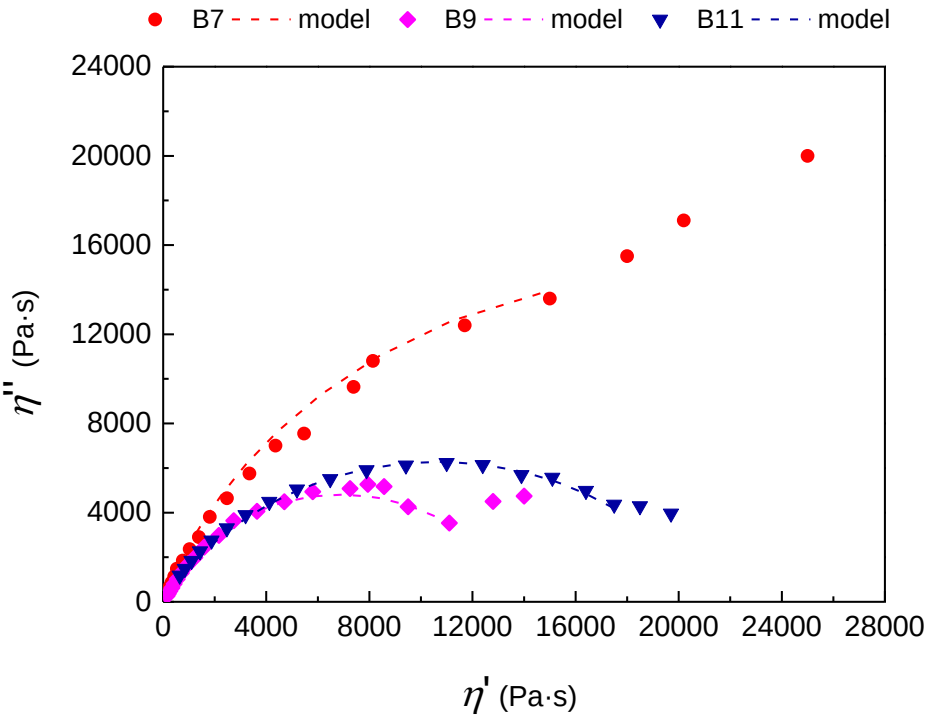

Figure 3. The Cole–Cole diagram of B7, B9, and B11. The relevant parts of the curves were fitted using the Cole–Cole model (dashed lines).

The data fitted with the model are shown in Figure 3, and the parameters of the model are summarized in Table 6. In Figure 3, the data exhibited a typical "shoulder" associated with the development of structures with longer relaxation times, including physical interactions,[45,46] indicating the existence of entanglements between the PMMA brushes present on the GO surface and the matrix PMMA chains. The evaluation of λ_0 confirmed the longest relaxation time observed in the case of sample B7, which was 1.35 s, while the composites B9 and B11 with shorter polymer chains showed λ_0 of 0.62 and 0.158 s, respectively.

Finally, the interpretation of *h* parameter was addressed. In essence, a lower *Đ* value of the polymers yields a lower *h* parameter. As shown by Garcia-Franco et al.,[43] polymers prepared by linear anionic polymerization (*Đ* below 1.1) exhibit *h* of around ~0.12, while polymers synthesized using metallocene gas phase catalysts (*Đ* around 2.4) possess *h* of ~0.35. In our case, the fitting procedure for B7 and Bí samples resulted to comparable *h* values, 0.275 and 0.288, which can be explained based on their similar *Đ* values. B11 exhibited h value rather higher, 0.321, that correlate with higher *Đ* determined from GPC analysis. Indeed, these values might be affected by the presence of GO-*g*-PMMA filler, but generally the data fall into *h* trends observed for the other systems.[43,45]

Table 6. Parameters of the Cole–Cole model of the GO-*g*-PMMA/PMMA composites.

Sample	η_0 (Pa·s)	λ_0 (s)	*h*
B7	48,300	1.35	0.275
B9	16,400	0.62	0.288
B11	21,315	0.158	0.321

The composites prepared via the "one-pot" strategy were finally compared to commercially available products. As reference material two different PMMAs were used. The molar mass M_n of PMMA1 was 31,500 g mol^{-1}, but *Đ* was broad at 6.67. The molar mass M_n of PMMA2 was 70,700 g mol^{-1} and *Đ* was 1.92. The M_n values of PMMA1 and PMMA2 were comparable to the freely dispersed PMMA chains of B11 and B7, respectively. In Figure 4a the storage modulus (*G'*) is compared. The *G'* values of both commercial PMMAs were comparable to B7 composites at temperatures below glass transition, that is, 113 °C. The composite B7 contained 10 wt % of filler, while B11 contained 14.2 wt % of the GO particles. Therefore, the *G'* of B11 was higher than that of B7, and this trend was visible in the whole temperature range. On the other hand, the commercial PMMA1composite with 10 wt % GO exhibited storage modulus values comparable to B11 below the glass transition region, i.e., to 100 °C. The reason was the presence of longer PMMA chains (M_w = 213,000 g mol^{-1}) than in the B7 composite. Above 100 °C, the *G'* of the PMMA1 composite dropped to the lowest values among all the investigated samples. This can be attributed to the lack of interaction between the filler

and matrix. Interestingly, the PMMA2 composite showed *G'* lower than the neat PMMA matrix. The reason can be attributed to the insufficient compatibility of filler and matrix.

The most significant difference between the commercial PMMA composites and the hybrid composite system was the shift in the glass transition temperature (T_g), as seen in Figure 4b. While the PMMA1 composite showed a T_g of 116 °C, the hybrid composites B7 and B11 showed significantly higher values, above 135 °C. This was almost a 20 °C difference. Thus, the prepared composites are clearly applicable to higher temperatures with retention of the mechanical properties.

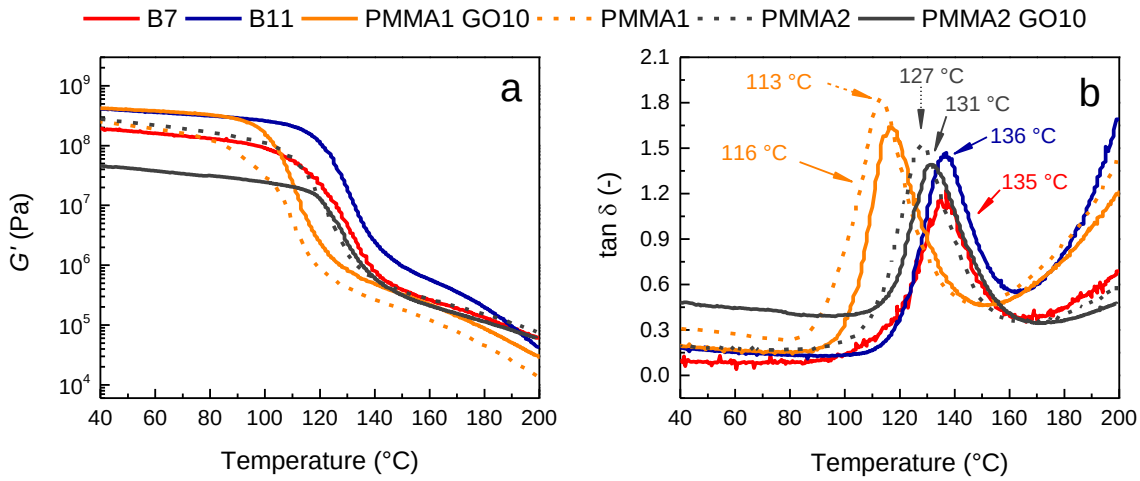

Figure 4. The temperature dependence of the (**a**) storage modulus (*G'*) and (**b**) damping factor (tanδ) of hybrid composites B7 and B11 compared to the commercial PMMA with 10 wt % GO.

Synthesis and properties of conductive GO-g-PSAN/PSAN composites

Statistical copolymers of styrene and acrylonitrile (SAN) are widely used in various applications, e.g., electronics, packaging, automotive and medical applications, because of their outstanding mechanical and chemical properties.[47] Therefore the same "one-pot" strategy was further applied for synthesis of SAN hybrids and composites. Compared to methyl methacrylate, the k_p of acrylonitrile monomer is even higher, 3560 L mol^{-1} s^{-1} at 25 °C.[48] However, copolymerization with a low k_p monomer, such as styrene with k_p = 340 L mol^{-1} s^{-1} at 60 °C,[33] can be utilized as a tool for efficient

tuning of the polymerization rate.[49] Thus the copolymerization can allow sufficient GO reduction without negative effect on molar mass and dispersity control.

In our previous work, the reduction of graphene oxide during the SI-ATRP of styrene was investigated.[27] Thus, the same reaction conditions were applied to prepare GO-*g*-SAN. Here, the catalyst consisting of PMDETA/CuBr was used. PMDETA is a more active ligand compared to the HMTETA that was used for methacrylate, while their ability to reduce graphene oxide particles is similar (Table 2). It should be pointed out that using an even more active ligand, such as Me_6TREN, led to uncontrolled polymerization, providing the copolymer with a dispersity over 4 (see Table S3). The monomer mixture of azeotropic composition (~ 39 mol % of AN) was chosen because it ensured no compositional drift during copolymerization.[50] Thus, the conversion of styrene was evaluated based on ^{1}H NMR, and conversion of AN was calculated according to the ratio of monomers in the azeotrope mixture. Control copolymerization without GO led to approximately 50% total monomer conversion after 48 h at 80 °C (Table 7, Entry C1). The narrow dispersity of SAN indicated that the polymerization was well controlled, and therefore the same reaction conditions were subsequently used for synthesis of the GO-*g*-SAN hybrid (Table 7, Entry C2). It can be clearly seen that the reduction was successful, and a high electrical conductivity of 0.4 S cm^{-1} was obtained for the hybrids after 48 h of polymerization.

The same reaction conditions were then applied in the preparation of the GO-*g*-SAN/SAN composites. Two composites with various feeds of GO contents, molar mass of the polymer chains, and conductivity were prepared (Table 7, Entries C3 and C4). In Entry C4, a bifunctional free initiator was used to prepare high molar mass of the SAN matrix. In this case the polymerization time was also increased to obtain conductive composites. Based on the monomer conversion the filler content in the final composites was calculated to be 5.3 wt % and 7.0 wt % for Entry C3 and Entry C4, respectively. In contrast to the GO-*g*-PMMA/PMMA composites, in the GO-*g*-SAN/SAN composites the filler content of 5.3 wt % was not sufficient to achieve the percolation threshold, and non-conductive composites were prepared. Increasing the filler content up to 7 wt %, however, provided

the GO-*g*-SAN/SAN composite with the same order of conductivity (10^{-6} S cm^{-1}) as achieved for the GO-g-PMMA/PMMA composite with similar filler content. This confirmed the applicability of the one-pot strategy to the preparation of conductive composites based on various vinyl polymers.

Table 7. Molar ratios of reagents, reaction conditions, monomer conversion determined by ^{1}H NMR; M_n and $Đ$ of free copolymers and electrical conductivity of hybrids (Entry C2) and composites (Entry C3, C4). In all reactions the molar ratios of CuBr:$CuBr_2$:PMDETA were 0.9:0.1:1; 66.7 vol % of anisole as solvent was used; 3.50×10^{-4} mol PMDETA/100 mg GO–Br was used; temperature was 80 °C.

Entry	Molar ratio		GO–Br [wt %]	Time [h]	Conv. [%]	M_n [g mol^{-1}]	$Đ$	Electrical conductivity [S cm^{-1}]
	St : AN	EBiB						
C1	200:130	1	0	48	50	19,800	1.01	NA
C2	200:130	0.89	0.9	48	30	12,000	1.02	0.43 ± 0.04
C3	100:65	0.89	1.8	48	33	12,900	1.14	$1.0\times10^{-12} \pm 7\times10^{-13}$
C4	100:65	0.44[a]	3.5	192	48	32,700	1.40	$5.4\times10^{-6} \pm 2.3\times10^{-8}$

[a] 2f-BiB was used; the molar ratio is related to the molar content of bromide groups.

The viscoelastic properties of the composites were investigated at 200 °C. In Figure 5a, the frequency dependence of the complex viscosity of the in situ composites C3 and C4 is shown. The C3 composite showed significantly lower viscosity than the C4 composite. The reasons were both the higher filler content and the higher length of polymer chains in the case of the C4 composite. Figure 5b shows the frequency dependence of storage modulus (*G'*) and loss modulus (*G''*). Both C3 and C4 exhibited liquid-like behavior in the whole frequency range, even though for the C4 composite the COP is visible at highest tested frequency of 50 Hz.

The properties of in situ prepared composites were further compared with the commercial SAN possessing a similar content of acrylonitrile (25 wt %) but a higher molar mass M_n of 66,000 g mol^{-1} ($Đ$ = 2.2) than the synthesized C3 and C4 composites. In Figure 6, the temperature sweep reveals

comparable storage modulus for composites C3, C4, and the commercial SAN with 9 wt % GO below T_g, i.e., to 112 °C, where the transition was observed for the neat SAN as well as the C3 composite. Composites with higher amounts of filler, ~7 wt %, showed the T_g at 120 °C.

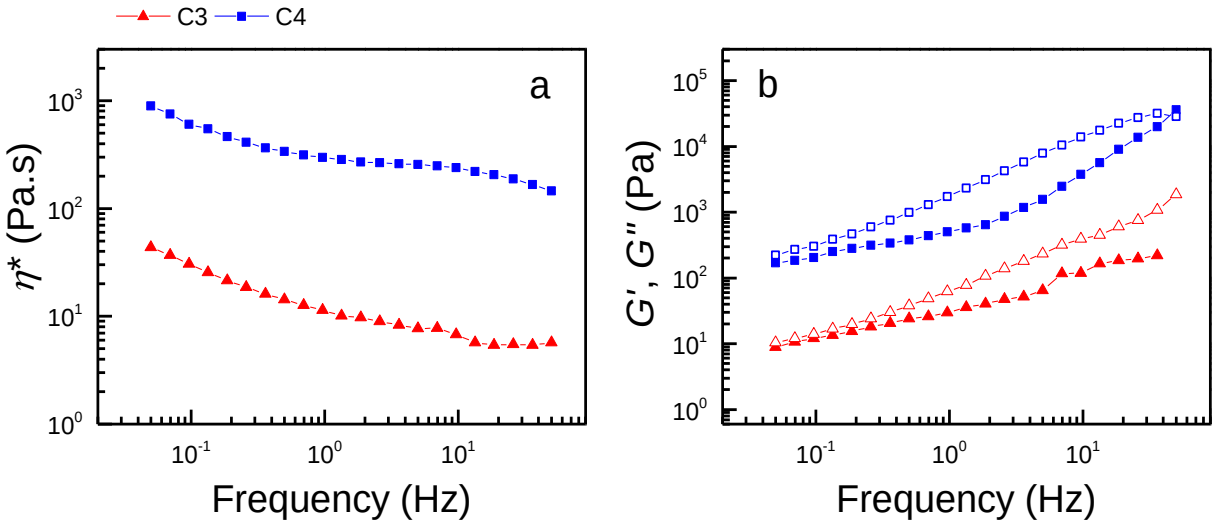

Figure 5. The viscoelastic properties of in situ prepared GO-*g*-SAN/SAN composites C3 and C4. Frequency dependence of (**a**) complex viscosity, and (**b**) storage and loss modulus measured at 200 °C.

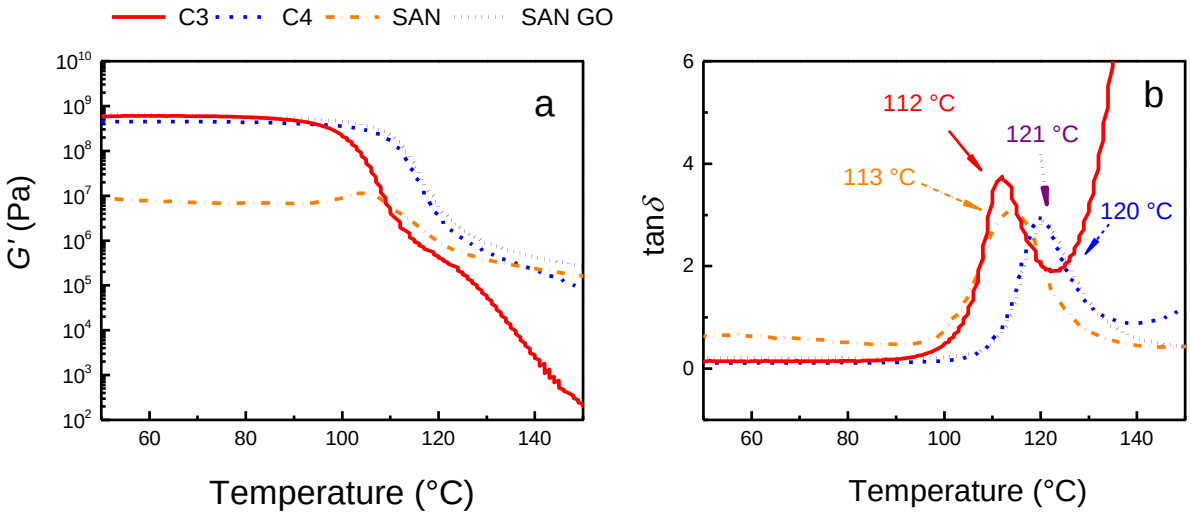

Figure 6. The temperature dependence of (**a**) storage modulus (*G'*) and (**b**) damping factor (tanδ) of in situ prepared GO-*g*-SAN/SAN composites C3 and C4 and comparison to commercial SAN and SAN with 9 wt % GO.

Both non-conductive and electrically conductive GO-*g*-SAN/SAN composites with good mechanical properties were expediently prepared. The results showed that the mechanical and electrical properties of graphene oxide-based composites can be finely tuned by the choice of conditions for ATRP. The "one-pot" synthetic approach allows a simple preparation method for composites with electrical conductivity values and mechanical properties suitable for electromagnetic interference (EMI) shielding and sensor applications.[4]

CONCLUSIONS

In this work, it was shown that GO can be reduced using tertiary amines containing short aliphatic substituents, enabling nucleophilic attack on carbon-bearing hydroxyl groups at the GO surface, leading to the decrease of oxygen groups at the surface and restoration of aromatic graphene structure. This was accompanied by the increase of electrical conductivity by 8 orders of magnitude. In contrast, GO reduction was not achieved using aromatic tertiary amines because of the steric hinderance. The reduction did not proceed at temperatures of 50 °C or lower. Using the excess of aliphatic tertiary amine-based ATRP ligands during ATRP allowed simultaneous reduction and modification of GO by surface-initiated ATRP. It was shown that the structure of the aliphatic amine-based ATRP ligand can be specifically selected for monomers with varied propagation rate coefficients, including methyl methacrylate and styrene in a mixture with acrylonitrile, in order to tune both polymerization rate and degree of GO reduction. Thus, GO-*g*-PMMA and GO-g-SAN hybrids with electrical conductivity in the range of 10^{-8} to 10^{0} S cm^{-1} were prepared. Finally, the "one-pot" strategy for preparation of graphene oxide copolymer composites with finely tunable mechanical properties and electrical conductivity was developed. The ratio of monomers and functionality of sacrificial initiator provided a tool for adjusting the length of polymer chains and, thus, the level of entanglements within the grafted chains and polymer matrix. These parameters, together with filler content, then determined the mechanical and viscoelastic properties of the composites and enabled their gentle tailoring. The general applicability of our strategy was proved by preparation of PMMA/GO-g-PMMA and

SAN/GO-g-SAN composites, while their electrical conductivity could be tailored in the range of 10^{-14} to 10^{-4} S cm^{-1}. We believe that this approach opens new pathways for precise composite design.

Supporting Information. Characterization methods, electrical conductivity of GO reduced with various amines and some GO hybrids, representative GPC spectra, Raman, FTIR and TGA of some hybrids and composites. This material is available free of charge via the Internet at http://pubs.acs.org.

AUTHOR INFORMATION

Corresponding Authors

E-mail: marketa.ilcikova@savba.sk (M. Ilcikova); jaroslav.mosnacek@savba.sk (J. Mosnáček); joanna.pietrasik@p.lodz.pl (J. Pietrasik)

Author Contributions

The manuscript was written with the contributions of all authors. All authors have given approval to the final version of the manuscript. The authors declare no competing financial interest.

ACKNOWLEDGMENTS

The authors thank National Science Centre, Poland, for their financial support through POLONEZ (UMO-2016/23/P/ST5/02131), which received funding from the European Union's Horizon 2020 research and innovation program under Marie Sklodowska-Curie grant agreement No. 665778. This work was supported by the Ministry of Education, Youth and Sports of the Czech Republic—DKRVO (RP/CPS/2020/003). This study was also performed during the implementation of the project Building-up Centre for advanced materials application of the Slovak Academy of Sciences, ITMS project code 313021T081, supported by Research & Innovation Operational Program funded by the ERDF. J.M. acknowledges project VEGA 2/0129/19 and together with M.I. acknowledge project APVV-19-0338 for financial support.

REFERENCES

(1) Mohd Radzuan, N. A.; Sulong, A. B.; Sahari, J. A Review of Electrical Conductivity Models for Conductive Polymer Composite. *Int. J. Hydrogen Energy* **2017**, *42* (14), 9262–9273. https://doi.org/10.1016/j.ijhydene.2016.03.045.

(2) Al-Saleh, M. H.; Sundararaj, U. A Review of Vapor Grown Carbon Nanofiber/Polymer Conductive Composites. *Carbon N. Y.* **2009**, *47* (1), 2–33. https://doi.org/10.1016/j.carbon.2008.09.039.

(3) Zhang, W.; Dehghani-Sanij, A. A.; Blackburn, R. S. Carbon Based Conductive Polymer Composites. In *Journal of Materials Science*; Springer, 2007; Vol. 42, pp 3408–3418. https://doi.org/10.1007/s10853-007-1688-5.

(4) Pang, H.; Xu, L.; Yan, D. X.; Li, Z. M. Conductive Polymer Composites with Segregated Structures. *Prog. Polym. Sci.* **2014**, *39* (11), 1908–1933. https://doi.org/10.1016/j.progpolymsci.2014.07.007.

(5) Kaur, G.; Adhikari, R.; Cass, P.; Bown, M.; Gunatillake, P. Electrically Conductive Polymers and Composites for Biomedical Applications. *RSC Adv.* **2015**, *5*, 37553–37567. https://doi.org/10.1039/c5ra01851j.

(6) Duan, L.; D'hooge, D. R.; Cardon, L. Recent Progress on Flexible and Stretchable Piezoresistive Strain Sensors: From Design to Application. *Prog. Mater. Sci.* **2020**, *114*, 100617. https://doi.org/10.1016/J.PMATSCI.2019.100617.

(7) Kou, Y.; Cheng, X.; Macosko, C. W. Polymer/Graphene Composites via Spinodal Decomposition of Miscible Polymer Blends. *Macromolecules* **2019**, *52* (20), 7625–7637. https://doi.org/10.1021/acs.macromol.9b01391.

(8) Folorunso, O.; Hamam, Y.; Sadiku, R.; Ray, S. S.; Joseph, A. G. Parametric Analysis of

Electrical Conductivity of Polymer-Composites. *Polymers*. MDPI AG July 29, 2019, p 1250. https://doi.org/10.3390/polym11081250.

(9) Sattar, T. Current Review on Synthesis, Composites and Multifunctional Properties of Graphene. *Topics in Current Chemistry*. Springer International Publishing April 1, 2019, p 10. https://doi.org/10.1007/s41061-019-0235-6.

(10) Smith, A. T.; LaChance, A. M.; Zeng, S.; Liu, B.; Sun, L. Synthesis, Properties, and Applications of Graphene Oxide/Reduced Graphene Oxide and Their Nanocomposites. *Nano Mater. Sci.* **2019**, *1* (1), 31–47. https://doi.org/10.1016/j.nanoms.2019.02.004.

(11) Zhu, Y.; Murali, S.; Cai, W.; Li, X.; Suk, J. W.; Potts, J. R.; Ruoff, R. S. Graphene and Graphene Oxide: Synthesis, Properties, and Applications. *Adv. Mater.* **2010**, *22* (35), 3906–3924. https://doi.org/10.1002/adma.201001068.

(12) Pei, S.; Cheng, H. M. The Reduction of Graphene Oxide. *Carbon N. Y.* **2012**, *50* (9), 3210–3228. https://doi.org/10.1016/j.carbon.2011.11.010.

(13) Aunkor, M. T. H.; Mahbubul, I. M.; Saidur, R.; Metselaar, H. S. C. The Green Reduction of Graphene Oxide. *RSC Advances*. Royal Society of Chemistry 2016, pp 27807–27825. https://doi.org/10.1039/c6ra03189g.

(14) Abdelhalim, A. O. E.; Sharoyko, V. V.; Meshcheriakov, A. A.; Martynova, S. D.; Ageev, S. V.; Iurev, G. O.; Al Mulla, H.; Petrov, A. V.; Solovtsova, I. L.; Vasina, L. V.; Murin, I. V.; Semenov, K. N. Reduction and Functionalization of Graphene Oxide with L-Cysteine: Synthesis, Characterization and Biocompatibility. *Nanomedicine Nanotechnology, Biol. Med.* **2020**, *29*, 102284. https://doi.org/10.1016/j.nano.2020.102284.

(15) Joshi, S.; Siddiqui, R.; Sharma, P.; Kumar, R.; Verma, G.; Saini, A. Green Synthesis of Peptide Functionalized Reduced Graphene Oxide (RGO) Nano Bioconjugate with Enhanced Antibacterial Activity. *Sci. Rep.* **2020**, *10* (1), 1–11. https://doi.org/10.1038/s41598-020-

66230-3.

(16) Yang, J.; Yan, X.; Chen, F.; Fan, P.; Zhong, M. Graphite Oxide Platelets Functionalized by Poly(Ionic Liquid) Brushes and Their Chemical Reduction. *J. Nanoparticle Res.* **2013**, *15* (1), 1–12. https://doi.org/10.1007/s11051-012-1383-6.

(17) Mirza-Aghayan, M.; Molaee Tavana, M.; Boukherroub, R. Sulfonated Reduced Graphene Oxide as a Highly Efficient Catalyst for Direct Amidation of Carboxylic Acids with Amines Using Ultrasonic Irradiation. *Ultrason. Sonochem.* **2016**, *29*, 371–379. https://doi.org/10.1016/j.ultsonch.2015.10.009.

(18) Vallés, C.; Papageorgiou, D. G.; Lin, F.; Li, Z.; Spencer, B. F.; Young, R. J.; Kinloch, I. A. PMMA-Grafted Graphene Nanoplatelets to Reinforce the Mechanical and Thermal Properties of PMMA Composites. *Carbon N. Y.* **2020**, *157*, 750–760. https://doi.org/10.1016/j.carbon.2019.10.075.

(19) Vuluga, D.; Thomassin, J. M.; Molenberg, I.; Huynen, I.; Gilbert, B.; Jérôme, C.; Alexandre, M.; Detrembleur, C. Straightforward Synthesis of Conductive Graphene/Polymer Nanocomposites from Graphite Oxide. *Chem. Commun.* **2011**, *47* (9), 2544–2546. https://doi.org/10.1039/c0cc04623j.

(20) Ilčíková, M.; Mrlík, M.; Sedláček, T.; Šlouf, M.; Zhigunov, A.; Koynov, K.; Mosnáček, J. Synthesis of Photoactuating Acrylic Thermoplastic Elastomers Containing Diblock Copolymer-Grafted Carbon Nanotubes. *ACS Macro Lett.* **2014**, *3* (10), 999–1003. https://doi.org/10.1021/mz500444m.

(21) Huang, C.-F. Surface-Initiated Atom Transfer Radical Polymerization for Applications in Sensors, Non-Biofouling Surfaces and Adsorbents. *Polym. J. 2016 484* **2016**, *48* (4), 341–350. https://doi.org/10.1038/pj.2016.24.

(22) Chen, J. K.; Hsieh, C. Y.; Huang, C. F.; Li, P. min. Characterization of Patterned

Poly(Methyl Methacrylate) Brushes under Various Structures upon Solvent Immersion. *J. Colloid Interface Sci.* **2009**, *338* (2), 428–434. https://doi.org/10.1016/J.JCIS.2009.06.040.

(23) Huang, C. F.; Chen, J. K.; Tsai, T. Y.; Hsieh, Y. A.; Andrew Lin, K. Y. Dual-Functionalized Cellulose Nanofibrils Prepared through TEMPO-Mediated Oxidation and Surface-Initiated ATRP. *Polymer (Guildf).* **2015**, *72*, 395–405. https://doi.org/10.1016/J.POLYMER.2015.02.056.

(24) Galeziewska, M.; Lipinska, M.; Mrlik, M.; Ilcikova, M.; Gajdosova, V.; Slouf, M.; Achbergerová, E.; Musilová, L.; Mosnacek, J.; Pietrasik, J. Polyacrylamide Brushes with Varied Morphologies as a Tool for Control of the Intermolecular Interactions within EPDM/MVQ Blends. *Polymer (Guildf).* **2021**, *215*, 123387. https://doi.org/10.1016/J.POLYMER.2021.123387.

(25) Choi, J.; Hore, M. J. A.; Clarke, N.; Winey, K. I.; Composto, R. J. Nanoparticle Brush Architecture Controls Polymer Diffusion in Nanocomposites. *Macromolecules* **2014**, *47* (7), 2404–2410. https://doi.org/10.1021/MA500235V.

(26) Chen, Z.; Xie, L.; Huang, X.; Li, S.; Jiang, P. Achieving Large Dielectric Property Improvement in Polymer/Carbon Nanotube Composites by Engineering the Nanotube Surface via Atom Transfer Radical Polymerization. *Carbon N. Y.* **2015**, *95*, 895–903. https://doi.org/10.1016/J.CARBON.2015.09.020.

(27) Ilčíková, M.; Mrlík, M.; Špitalský, Z.; Mičušík, M.; Csomorová, K.; Sasinková, V.; Kleinová, A.; Mosnáček, J. A Tertiary Amine in Two Competitive Processes: Reduction of Graphene Oxide vs. Catalysis of Atom Transfer Radical Polymerization. *RSC Adv.* **2015**, *5* (5), 3370–3376. https://doi.org/10.1039/c4ra12915f.

(28) Mrlík, M.; Ilčíková, M.; Plachý, T.; Pavlínek, V.; Špitalský, Z.; Mosnáček, J. Graphene Oxide Reduction during Surface-Initiated Atom Transfer Radical Polymerization of Glycidyl Methacrylate: Controlling Electro-Responsive Properties. *Chem. Eng. J.* **2016**, *283*, 717–720.

https://doi.org/10.1016/j.cej.2015.08.013.

(29) Kutalkova, E.; Mrlik, M.; Ilcikova, M.; Osicka, J.; Sedlacik, M.; Mosnacek, J. Enhanced and Tunable Electrorheological Capability Using Surface Initiated Atom Transfer Radical Polymerization Modification with Simultaneous Reduction of the Graphene Oxide by Silyl-Based Polymer Grafting. *Nanomaterials* **2019**, *9* (2), 308. https://doi.org/10.3390/nano9020308.

(30) Jankovský, O.; Marvan, P.; Nováček, M.; Luxa, J.; Mazánek, V.; Klímová, K.; Sedmidubský, D.; Sofer, Z. Synthesis Procedure and Type of Graphite Oxide Strongly Influence Resulting Graphene Properties. *Appl. Mater. Today* **2016**, *4*, 45–53. https://doi.org/10.1016/j.apmt.2016.06.001.

(31) Kirkpatrick, S. Percolation Ancl Conduction. *Rev. Mod. Phys.* **1973**, *45* (4), 574–588.

(32) Buback, M.; Gilbert, R. G.; Hutchinson, R. A.; Klumperman, B.; Kuchta, F.-D.; Manders, B. G.; O'Driscoll, K. F.; Russell, G. T.; Schweer, J. Critically Evaluated Rate Coefficients for Free-Radical Polymerization, 1. Propagation Rate Coefficient for Styrene. *Macromol. Chem. Phys.* **1995**, *196* (10), 3267–3280. https://doi.org/10.1002/macp.1995.021961016.

(33) Odian, G. Radical Chain Polymerization. In *Principles of Polymerization*; John Wiley & Sons, Inc.: Hoboken, New Jersey, 2004; pp 198–349. https://doi.org/10.1002/047147875x.ch3.

(34) Beuermann, S.; Buback, M.; Hesse, P.; Kuchta, F. D.; Lacík, I.; Van Herk, A. M. Critically Evaluated Rate Coefficients for Free-Radical Polymerization. Part 6: Propagation Rate Coefficient of Methacrylic Acid in Aqueous Solution - (IUPAC Technical Report). *Pure Appl. Chem.* **2007**, *79* (8), 1463–1469. https://doi.org/10.1351/pac200779081463.

(35) Tang, W.; Kwak, Y.; Braunecker, W.; Tsarevsky, N. V.; Coote, M. L.; Matyjaszewski, K. Understanding Atom Transfer Radical Polymerization: Effect of Ligand and Initiator

Structures on the Equilibrium Constants. *J. Am. Chem. Soc.* **2008**, *130* (32), 10702–10713. https://doi.org/10.1021/JA802290A.

(36) Thermo Fisher Scientific, Thermo Avantage Software 5.9922, XPS Knowledge Database.

(37) Queffelec, J.; Gaynor, S. G.; Matyjaszewski, K. Optimization of Atom Transfer Radical Polymerization Using Cu(I)/Tris(2-(Dimethylamino)Ethyl)Amine as a Catalyst. *Macromolecules* **2000**, *33* (23), 8629–8639. https://doi.org/10.1021/ma000871t.

(38) Matyjaszewski, K. Atom Transfr Radical Polymerization (ATRP): Current Status and Future Perspectives. *Macromolecules* **2012**, *45* (10), 4015–4039. https://doi.org/10.1021/ma3001719.

(39) Matyjaszewski, K.; Tsarevsky, N. V. Macromolecular Engineering by Atom Transfer Radical Polymerization. *J. Am. Chem. Soc.* **2014**, *136* (18), 6513–6533. https://doi.org/10.1021/ja408069v.

(40) Tang, H.; Shen, Y.; Li, B.-G.; Radosz, M. Tertiary Amine - Enhanced Activity of ATRP Catalysts CuBr/TPMA and CuBr/Me $_6$ TREN. *Macromol. Rapid Commun.* **2008**, *29* (22), 1834–1838. https://doi.org/10.1002/marc.200800378.

(41) Hayashida, K.; Tanaka, H. Ultrahigh Electrical Resistance of Poly(Cyclohexyl Methacrylate)/Carbon Nanotube Composites Prepared Using Surface-Initiated Polymerization. *Adv. Funct. Mater.* **2012**, *22* (11), 2338–2344. https://doi.org/10.1002/adfm.201103089.

(42) Gao, X.; Feng, W.; Zhu, S.; Sheardown, H.; Brash, J. L. Kinetic Modeling of Surface-Initiated Atom Transfer Radical Polymerization. *Macromol. React. Eng.* **2010**, *4* (3–4), 235–250. https://doi.org/10.1002/MREN.200900063.

(43) Garcia-Franco, C. A.; Mead, D. W. Rheological and Molecular Characterization of Linear Backbone Flexible Polymers with the Cole-Cole Model Relaxation Spectrum. *Rheol. Acta*

1999, *38*, 34–47. https://doi.org/10.1007/s003970050154.

(44) Ghasemi, I.; Azizi, H.; Naeimian, N. Rheological Behaviour of Polypropylene/Kenaf Fibre/Wood Flour Hybrid Composite. *Iran. Polym. J. (English Ed.* **2008**, *17* (3), 191–198.

(45) Cvek, M.; Kracalik, M.; Sedlacik, M.; Mrlik, M.; Sedlarik, V. Reprocessing of Injection-Molded Magnetorheological Elastomers Based on TPE Matrix. *Compos. Part B Eng.* **2019**, *172*, 253–261. https://doi.org/10.1016/j.compositesb.2019.05.090.

(46) Ilcikova, M.; Zygo, M.; Mrlik, M.; Osicka, J.; Masar, M.; Slouf, M.; Maslowski, M.; Kracalik, M.; Pietrasik, R.; Mosnacek, J.; Pietrasik, J. The Effect of Short Polystyrene Brushes Grafted from Graphene Oxide on the Behavior of Miscible PMMA/SAN Blends. *Polymer (Guildf).* **2020**, *211*, 123088. https://doi.org/10.1016/j.polymer.2020.123088.

(47) Shanmugharaj, A. M.; Bae, J. H.; Nayak, R. R.; Ryu, S. H. Preparation of Poly(Styrene-Co-Acrylonitrile)-Grafted Multiwalled Carbon Nanotubes via Surface-Initiated Atom Transfer Radical Polymerization. *J. Polym. Sci. Part A Polym. Chem.* **2007**, *45* (3), 460–470. https://doi.org/10.1002/pola.21858.

(48) Junkers, T.; Koo, S. P. S.; Barner-Kowollik, C. Determination of the Propagation Rate Coefficient of Acrylonitrile. *Polym. Chem.* **2010**, *1* (4), 438–441. https://doi.org/10.1039/c0py00019a.

(49) Pietrasik, J.; Dong, H.; Matyjaszewski, K. Synthesis of High Molecular Weight Poly(Styrene-Co-Acrylonitrile) Copolymers with Controlled Architecture. *Macromolecules* **2006**, *39* (19), 6384–6390. https://doi.org/10.1021/ma0611927.

(50) Tsarevsky, N. V; Sarbu, T.; Go, B.; Matyjaszewski, K. Synthesis of Styrene-Acrylonitrile Copolymers and Related Block Copolymers by Atom Transfer Radical Polymerization. *Macromolecules* **2002**, *35* (16), 6142–6148. https://doi.org/10.1021/ma020560d.